ORIGINAL ARTICLE

CYTOMETRY
Journal of Quantitative Cell Science PART A

Quantitative Imaging of B1 Cyclin Expression Across the Cell Cycle Using Green Fluorescent Protein Tagging and Epifluorescence

Arnica Karuna,[1*] Francesco Masia,[1,2] Sally Chappell,[3] Rachel Errington,[3] Andrew M. Hartley,[2] Darran Dafydd Jones,[2] Paola Borri,[2] Wolfgang Langbein[1]

[1]School of Physics and Astronomy, Cardiff University, Cardiff, UK

[2]School of Biosciences, Cardiff University, Cardiff, UK

[3]School of Medicine, Cardiff University, Cardiff, UK

Received 20 November 2019; Revised 21 April 2020; Accepted 28 April 2020

Grant sponsor: Cardiff University; Grant sponsor: Engineering and Physical Sciences Research Council, Grant numbers: EP/I005072/1, EP/J015318/1; Grant sponsor: Leverhulme Trust, Grant number: LT20085; Grant sponsor: Biotechnology and Biological Sciences Research Council, Grant numbers: BB/H003746/1, BB/M000249/1; Grant sponsor: Cardiff SynBio Initiative/SynBioCite

*Correspondence to: Arnica Karuna, Friedrich Schiller University, Jena, Germany Email: arnica.karuna@uni-jena.de

Present address of Andrew M. Hartley, School of Biomedical Sciences, Astbury Centre for Structural Biology, University of Leeds, Leeds, UK.

Published online 1 July 2020 in Wiley Online Library (wileyonlinelibrary.com)

DOI: 10.1002/cyto.a.24038

Abstract

In this article, we report the number of cyclin B1 proteins tagged with enhanced green fluorescent protein (eGFP) in fixed U-2 OS cells across the cell cycle. We use a quantitative analysis of epifluorescence to determine the number of eGFP molecules in a nondestructive way, and integrated over the cell we find 10^4 to 10^5 molecules. Based on the measured number of eGFP tagged cyclin B1 proteins, knowledge of cyclin B1 dynamics through the cell cycle, and the cell morphology, we identify the stages of cells in the cell cycle. © 2020 The Authors. *Cytometry Part A* published by Wiley Periodicals LLC. on behalf of International Society for Advancement of Cytometry.

Key terms

fluorescence microscopy; fluorophore concentration; U-2 OS cells; cyclin B1-eGFP

OPTICAL microscopy techniques (1–3) are of fundamental importance to advance our understanding of biological systems. Tools such as phase contrast, differential interference contrast (DIC), and fluorescence microscopy are in widespread use in bioimaging applications. While not chemically specific, quantitative phase contrast (4–7) and DIC (8,9) can be used, apart from structural investigations, to quantitatively determine dry mass distribution in cell biology studies. On the other hand, fluorescence based methods which are chemically specific due to the selectivity of fluorophore binding sites can be applied in several ways, some of them offering super-resolution down to the 10 nm range. In its simplest form, fluorescence microscopy is implemented in a widefield microscope with a lamp as the light source. To obtain 3D sectioning, confocal laser scanning can be used, for example, to study the cell cycle (10,11). Furthermore, two-photon laser scanning fluorescence (12–14) and fluorescence lifetime imaging microscopy (15) have been used to study cellular processes like protein interactions and metabolism (16). Despite the associated challenges of photobleaching and phototoxicity, fluorescence microscopy tools form the basis of a large fraction of studies in biology (17), motivated by the high contrast and the past development providing a tool-set of specific fluorophores.

Fluorescence was used in the past to quantify protein numbers and concentrations in cells (18). Specifically, tagging with green fluorescent protein was calibrated using rotavirus-derived virus-like particles (19), and different proteins were quantified in yeast using yellow fluorescent protein tagging (20), using immunoblotting for calibration.

Cell division is a critical fundamental biological process essential to life as well as organism growth and repair. During cell division, the genetic material (21) and organelles (22,23) are replicated and distributed between the daughter cells. The cell

cycle broadly comprises two stages (24), interphase and mitosis. During interphase, the cell undergoes growth and synthesizes various biomolecules in preparation for mitosis. In the mitotic stage of the cell cycle, distribution of the genetic material and the organelles takes place, and thereafter, through cytokinesis, the cell divides into two genetically identical daughter cells. The progress of a cell through the cell cycle is mediated by cyclin-dependent kinases (CDKs) and cyclins. Binding of a specific cyclin to the CDK followed by phosphorylation of the CDK by a CDK activating kinase activates the CDK (24,25). Various CDK-cyclin complexes are activated at different stages of the cell cycle, with CDK 1-cyclin B driving the cell from the synthesis (S) phase of interphase to the mitotic (M) phase. In cancer cells, the CDK–cyclin control of the cell cycle is rendered dysfunctional. Therefore, by studying cyclins and CDKs or CDK-cyclin complexes, the cell cycle of cancers can be probed from a biochemical and cell biology point of view. Moreover, CDKs are also obvious targets of various anticancer drugs (26,27). Previously, flow cytometry readouts of fluorophores targeting various parts of the cell were studied in correlation with fluorescence microscopy images to reveal the specificity of a new monoclonal antibody, H3P mAb (28). In this extensive study, in addition to H3P mAb, conventional fluorophores such as DAPI, propidium iodide for DNA, and fluorescein for cyclins A and B1 were used to conclude that the developed antibody is highly specific to histone H3 phosphorylated at Ser-10. The quantitative results were drawn from flow cytometry while microscopy was used to correlate the morphology and origin of the fluorescence intensities within the cells.

In this article, we investigate cells expressing cyclin B1 genetically labeled with eGFP, and quantify the fluorescence imaging to determine the number of these molecules in the cell across the cell cycle. Notably, we use the known absorption cross section of eGFP to calibrate the number of molecules in a calibration sample, and then determine the fluorescence per molecule on this sample, to calibrate the fluorescence imaging. The quantification method demonstrated in this article can be applied to similar biomedically relevant studies, for example, to measure the concentrations of fluorophore target molecules or to reveal pharmacodynamics of various autofluorescent drugs.

Materials and Methods

Sample Preparation

Human osteosarcoma cells [U-2 OS] (GFP G2M P2B2) transfected with a G2M Cell Cycle Phase Marker (GE Healthcare, UK) were cultured (29) under standard tissue culture (TC) conditions. The cells were seeded on #1 coverslips placed into a single well of a multiwell plate and allowed to adhere, spread, and proliferate for 24 h, in complete TC media comprising McCoys media, 10% fetal bovine serum (FBS), penicillin/streptomycin, glutamine, and G418. To prepare 400 ml medium, we used 348 ml McCoys 5A media (Sigma M8403, UK), 40 ml FBS, 4 ml solution of 100× Penicillin/Streptomycin (Sigma P0781, UK), 4 ml 100× L-Glutamine (Sigma C5914, UK), and 4 ml G418 (50 mg/ml in water) (Sigma G8168, UK). The cells were washed with PBS and subsequently fixed for 30 min in BD-Cytofix (BD Biosciences, San Jose, CA), a mild fixative agent that prevents the denaturation of eGFP. Following preparation, the well plates were covered and kept refrigerated at 4°C until imaging. To mount the cells for imaging, approximately 13 µl PBS was pipetted into a well created by the 13 mm diameter opening of a 0.12 mm thick adhesive imaging spacer (Grace Biolabs Secure Seal, Bend, Oregon) on a microscope slide. The coverslip was then inverted over the medium-filled well on the slide and sealed, ready to be imaged. Since cyclin B is active in the mitotic stage of the cell cycle, fluorescence imaging of eGFP-B1 transfected cells enables accurate discrimination of the mitotic cells from interphase or quiescent cells on the coverslip. For quantitative reference, a calibration sample was prepared with approximately 10 µl of a 40 µM eGFP solution produced recombinantly, as described previously (30,31). The eGFP solution was pipetted to fill the 9 mm diameter opening of a 0.12 mm thick imaging spacer (Grace Biolabs Secure Seal, Bend, Oregon). A #1 coverslip was inverted over the spacer, creating a sealed well of eGFP.

Setup

The epifluorescence images used in this article were acquired on an inverted microscope (Nikon Ti-U) equipped with brightfield, DIC, and epifluorescence. We use a dry objective (Nikon MRD00205) of 0.75 numerical aperture (NA) and 20× magnification. For epifluorescence imaging, we used as the source of excitation a broadband metal-halide lamp (Prior Lumen 200). The emission of the lamp was filtered using a filter cube (Semrock GFP-A-Basic-NTE, comprising an exciter (FF01-469/35-25), an emitter (FF01-525/39-25), and a dichroic (FF497-Di01-25x36)). The cells were imaged using a monochrome CCD camera (Hamamatsu Orca) with 1,344 × 1,024 pixels of 6.45 µm size, 8 electrons (e) read noise and 18 ke full well capacity.

The absorption spectrum of the calibration sample was measured on a spectrometer (USB2000-FLG Ocean Optics) with an operation range of 380–1,050 nm. The light source in this setup was a lamp (HL-2000-FHSA Ocean Optics).

Results

To calibrate the fluorescence microscopy, we first measured the absorbance, A of the calibration sample using the relation

$$A = -\log_{10}\left(\frac{S-D}{R-D}\right), \tag{1}$$

where S is the transmission intensity spectrum of the calibration sample (eGFP), R is the transmission intensity spectrum of a reference sample prepared equal to the calibration sample but not containing eGFP, and D is the dark spectrum (taken with the lamp switched off). The resulting absorbance

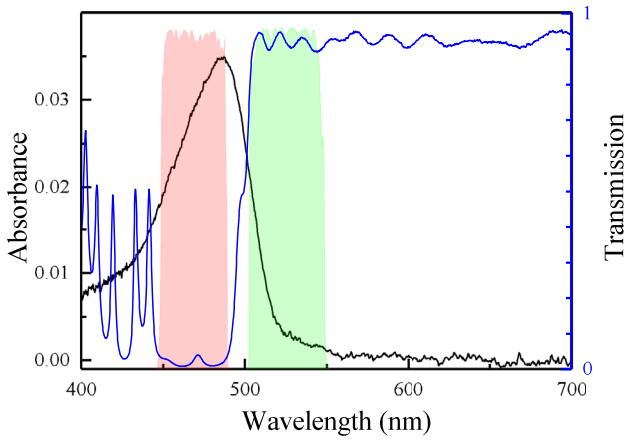

Figure 1. Absorbance spectrum of the calibration sample (black line). For comparison, the dichroic, exciter, and emitter transmission spectra specified by the manufacturer are shown in blue, red, and green, respectively. [Color figure can be viewed at wileyonlinelibrary.com]

spectrum of eGFP, with a maximum value 3.46% at a wavelength of $\lambda = 488$ nm is shown in Figure 1 as black line.

Using Lambert–Beer's law, $A = \varepsilon C l$, where ε is the molar extinction coefficient and l is the pathlength traveled by the incident light through the solution, the molar concentration C of eGFP in the solution can be determined. For eGFP at $\lambda = 488$ nm, we have $\varepsilon = 53{,}000\ \mathrm{M}^{-1}\ \mathrm{cm}^{-1}$ (32), and the pathlength l is 120.8 μm, measured using the microscope focusing stage while imaging with a water immersion objective (Nikon 60× 1.27NA, MRD70650). Due to the matching immersion and medium index, spherical errors are avoided and the focus motion in the sample is equal to the motion of the objective.

Using these values in Lambert–Beer's law, the concentration of eGFP in the solution is determined to be 54 ± 5 μM, considering 5% relative error in absorbance, 8% relative error (32) in ε, and 0.5% relative error in the pathlength. The number of eGFP molecules per area in the calibration sample, n, is then calculated using the relation $n = CN_A l$, where N_A is Avogadro's number. The error in n is dominated by the error in C, resulting in $n = (3.9 \pm 0.4) \times 10^{14}/\mathrm{cm}^2$. These values were then used to quantify the eGFP in cells. The epifluorescence images were analyzed in ImageJ (NIH) to calculate the sum of intensities, I_c of pixels enclosed within a contour defining the boundary of the cell. These intensities were then normalized with the fluorescence of the eGFP sample imaged under otherwise identical conditions to calculate the number of eGFP molecules in the cells given by

$$N_c = \frac{nI_c\tau_p A_0}{\bar{I}_p \tau_c}, \qquad (2)$$

where $\tau_p = 0.6$ ms and $\tau_c = 5$ s (unless otherwise specified) are the exposure times used to acquire the images of the eGFP sample and the cells, respectively. $\bar{I}_p = 2{,}385$ is the mean pixel intensity in counts measured over an area of the image of the pure eGFP sample and A_0 is the camera pixel area at the sample, equal to $0.104\ \mu\mathrm{m}^2$ for the 20×0.75NA objective used for the fluorescence imaging. The fluorescence emission of this sample showed a systematic variation of 6% standard deviation from its mean value across the field of view of the dry objective used for cell imaging. This variation is much smaller than the variations between cells and thus does not significantly affect the analysis. The illuminated size on the sample has about 1 mm diameter. The blurring of the edges of the field due to the depth of the sample is given by 120 μm × 0.75/1.33 = 68 μm, using the refractive index of water of 1.33, and is not affecting the center 0.5 mm of the field analyzed in this article.

The detection efficiency $E_D = T_o E_{CCD} F_\Omega = 3.1\%$ of the setup is determined by the transmission of the optics $T_o = 0.6$, the camera quantum efficiency $E_{CCD} = 0.6$, and the collected fraction of the full solid angle given by $F_\Omega = \Omega/(4\pi) = 8.7\%$ for 0.75NA in water of refractive index 1.33. The illumination intensity at the sample is estimated starting with the number of eGFP per camera pixel $N_p = nA_0 = 4.1 \times 10^5$. The photon emission rate per eGFP is then given by $\nu_e = \Gamma \bar{I}_p/(\tau_p N_p E_D) = 1{,}500$ Hz, using the camera gain, $\Gamma = 4.45$ electrons/count. The photon absorption rate is then given by $\nu_a = \nu_e/E_{eGFP} = 2{,}500$ Hz using the quantum efficiency $E_{eGFP} = 0.6$ of eGFP (31). The eGFP absorption cross section at $\lambda = 488$ nm is then calculated as $\sigma = \log(10)\varepsilon/N_A = 2.03 \times 10^{-16}\ \mathrm{cm}^2$, and the excitation intensity as $I = \nu_a hc/(\lambda\sigma) = 5.0\ \mathrm{W/cm}^2$.

After this calibration, we determined the spatially resolved eGFP densities across a large number of cells covering different stages across the cell cycle, and determined N_c integrating over the cell area. Background corrected images were used, where the background was determined as the mean pixel value over an area (~70 × 70 pixels) of the coverslip adjacent to but outside the cell. This was subtracted from each pixel of the cell image before calculating the number of molecules. In Figure 2, N_c is plotted against cell cycle stage identifier, showing a distribution in the range of 10^4 to 10^5 eGFP-cyclin B1 molecules per cell. The stage identifier is a number sorting the cells along the cell cycle, assigned using their morphology and their eGFP-cyclin B1 expression. For this assignment, we recall that cyclin B1 is produced during the S phase, in the rough endoplasmic reticulum. The metaphase promoting factor, which is cyclin B1 with CDK1, is localized in the cytosol during interphase (G_2) and gets transported to the nucleus before the disintegration of the nuclear envelope in prophase, marking the onset of mitosis (33). After the chromosome alignment on the metaphasic plate (34), cyclin B1 degradation begins. In the samples studied, the eGFP emission was accordingly found to be stronger either in the cytoplasmic or in the nuclear region of the cell, depending on the cell cycle stage.

In addition to the cell cycle stage dependent variation, the number of cyclin B1 molecules at each stage of the cell cycle varies also across the individuals of the cell population.

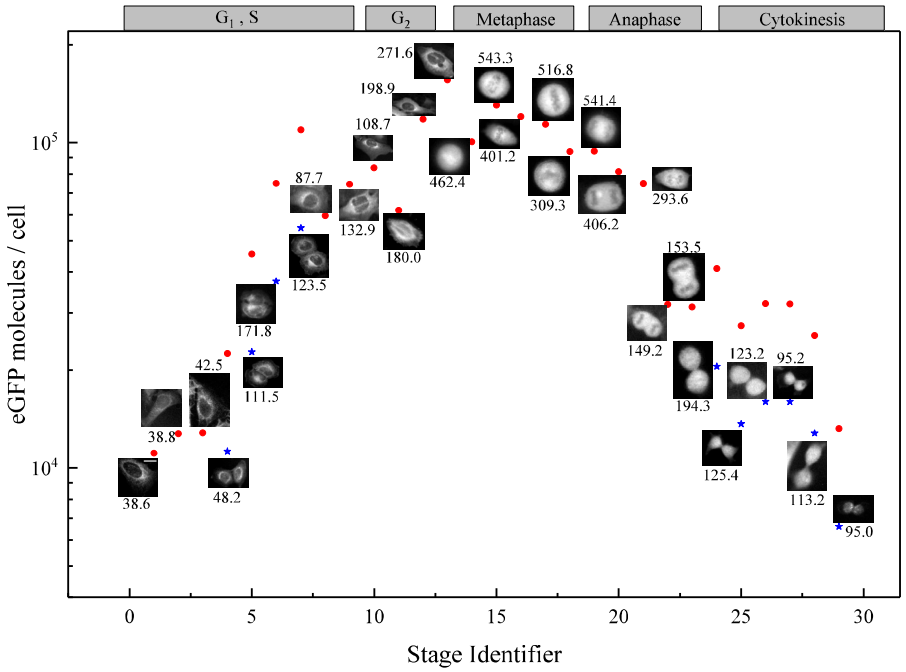

Figure 2. Quantitative analysis of eGFP expression along the cell cycle (images of cells are placed next to the data points). Cells 3, 6, 14, 18, 24, and 29 were imaged using 1.5 s exposure time. The scale bar shown on the first cell is 10 μm and is valid for all images shown in the plot. Data points indicated in red circles are the values over the cells, in some cases, over two cells. Data points represented by blue stars correspond to the images which show two cells almost completely separated cytoplasmically for which the number of eGFP molecules was evaluated across both the cells, and then divided by two. In these cases, the images of the cells have been placed near the blue stars to indicate the half value to be considered in analysis. The numbers next to the images give the maximum area concentration of the gray scale used (black [0] to white [maximum]), in units of molecules/μm^2. [Color figure can be viewed at wileyonlinelibrary.com]

Smith et al. have reported a typical relative decrease of eGFP-cyclin B1 expression of approximately 35% in U-2 OS cells in metaphase over two consecutive cell cycles (35). This inherent variation in cyclin B1 expression between cells makes it difficult to sort cells in broadly classified substages of interphase using the eGFP expression only.

For the analysis presented in this section, 29 epifluorescence images showing 39 fixed U-2 OS cells were selected. The selection was made to exclude cells on top of each other, and included those exhibiting different shapes and fluorescence intensities to ensure a broad population spread comprising individuals in various stages of the cell cycle. For the images containing two cells, we assume the cells to be in the same stage. The cell stage identifiers were assigned to the epifluorescence images using the eGFP localization according to Table 1, number of molecules (calculated using Equation 2) and by identifying the morphological features of the cells at various stages of the cell cycle, considering the spatial distribution of eGFP in the cells. The numbering of the cell cycle stage is aligned chronologically along the cell cycle, starting with interphase. In the following discussion, we refer to the cells and their images using their stage identifier number. In this method, we sorted the cells first into interphase and the substages of mitosis by observing their morphology. Flat cells were designated as interphase cells while the cells showing a spherical morphology were considered mitotic. Within mitosis, the cell morphology changes from metaphase to cytokinesis, which was taken into account. Finally, within the identified stages, the cells were arranged in either increasing or decreasing order of the number of eGFP molecules according to the expected trend relative to cells in metaphase. In the leading and trailing regions of the curve shown in Figure 2, we observe that the daughter cells which appear attached to each other (cells 4–7, 9, and 11) with or without apparent cytoplasmic division, are given lower identifier numbers than cell 29 which appears to be in early stages of cytokinesis. This was done due to the higher number of eGFP molecules in this set of cells compared to cell 29, relying on the knowledge that cyclin B1 levels reach a maximum in metaphase following which they decline

Table 1. Localization of cyclin B1-eGFP throughout the cell cycle in fixed cells (33,34,36)

CELL CYCLE STAGE	CYCLIN B1-EGFP LOCALIZATION
Interphase (S, G_2)	Cytosol, microtubules
Late G_2	Cytosol, centrosomes
Prophase	Nucleus
Prometaphase	Spindles
Late metaphase onwards	Progressive degradation

(cyclin B1 expression is actually the net rate of production of the protein, but the expression level refers to the number of proteins, represented here by the fluorescence intensity of the eGFP attached to the protein). While the number of eGFP molecules in cell 14 is lower than that of cells 12 and 13, cell 14 is given a higher identifier number due to its mitotic morphology. Such correlations were applied over the entire set of cells imaged and the resulting plot given in Figure 2 shows the variation of the number of cyclin B1 molecules via the number of eGFP molecules per cell, over various cells fixed in different stages of the cell cycle. We have included cells showing the weakest fluorescence, which are in G_1/S, to provide an upper limit for the autofluorescence of the cells. The graph shows that the eGFP number increases by an order of magnitude to about 10^5 molecules/cell as the cells approach mitosis, peaks at metaphase and progressively declines thereafter until the next cell cycle commences.

The maximum areal number density of eGFP molecules given in the image scaling shown in Figure 2 is calculated as

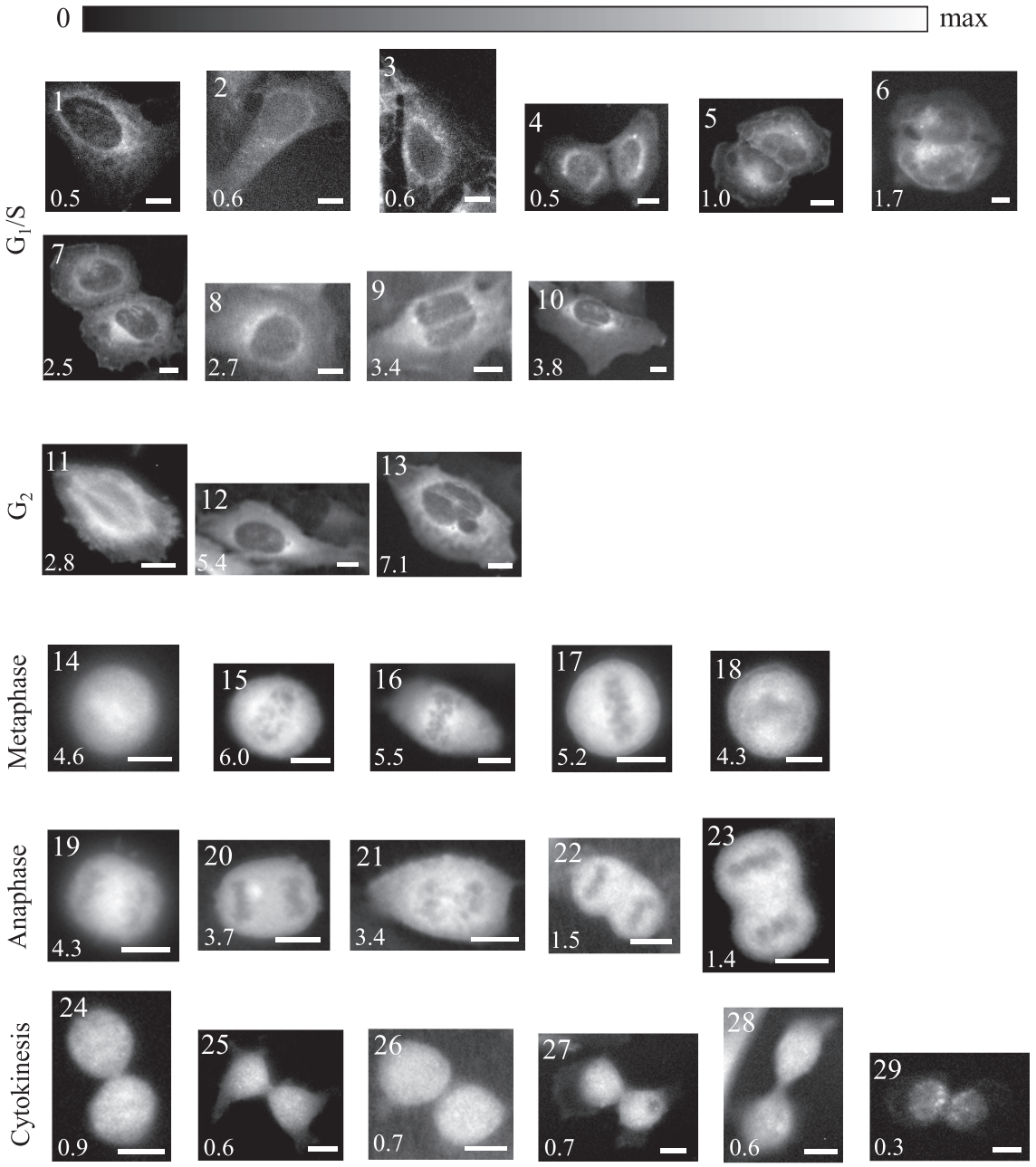

Figure 3. Epifluorescence images of the cells shown in Figure 2 arranged in order of increasing stage identifier (indicated top left of each image) from left to right in each stage of the cell cycle (top to bottom). The numbers on bottom left of the images are the detected photoelectron rates from the cell in MHz. The scale bars shown are 10 μm.

$n_{max} = nI_{max}\tau_p/(\bar{I}_p\tau_c)$, where I_{max} is the maximum pixel value within the cell area. The result of this analysis is an eGFP expression during the cell cycle which is consistent with the known behavior of cyclin B1 (see Table 1). Using a cell volume of 4,000 μm^3 (37), the molar concentration of eGFP in mitotic cells with 1.3×10^5 eGFP molecules is 54 nM. High-resolution images of the cells, of which thumbnails are given adjacent to the data points in Figure 2, are shown in Figure 3 to display clearly the cell morphologies. The total number of photoelectrons detected per second over each cell is also given, calculated as $N_{pe} = \Gamma I_c/\tau_c$. Previously, confocal fluorescence was used to measure cyclin B GFP expression by mRNA injection in starfish oocytes (38). The endogenous concentration was estimated to be 20 nM using the effect of the expression on the germinal vesicle breakdown timing. This is close to the concentration we have determined in our analysis of U-2 OS cells.

In literature, a 1:1 correspondence between the numbers of eGFP and cyclin B1 molecules in U-2 OS cells has been reported (39) using flow cytometry. Specifically, in G_1 cells, 2,500 and in G_2 cells, 7,000 molecules of eGFP-cyclin B1 were calculated (39). It is expected that the number of eGFP and cyclin B1 molecules will increase in the subsequent mitotic stages. In comparison to these values on live cells, we obtain for fixed cells, molecule numbers of the order of $(0.9–5) \times 10^4$ in G_1 and G_2 and around 10^5 in the mitotic stage of the cell cycle. The differences in the results could be related to the variability in the cyclin B1 expression across different cells in a population and over subsequent cell cycles. Additionally, differences in the number of molecules of cyclin B1 in HeLa cells depending on the counting method used have been reported (40), where the results of quantitative Western blotting of HeLa cells indicate cyclin B1 molecule numbers/cell of a few 10^6, consistent with another study (41). However, the results in these two publications are 2–3 orders of magnitude higher than those reported by Arooz et al. (42). Since all three studies use Western blotting, it is possible that these variations are due to biological reasons or sample preparation methods as indicated by Frisa et al. (40).

In contrast to Western blotting and flow cytometry (which are also technically invasive and complex) the presented method using epifluorescence imaging is a relatively fast, direct, and simple technique which facilitates eGFP-cyclin B1 concentration determination, requiring only conventional and readily available optical microscopy components. Our results are in between those in literature (39–42). We note that our method is sensitive to the following issues identified previously (18): (i) Autofluorescence—which we have estimated by analyzing the cells of weakest fluorescence. They show equivalent emission of around 10^4 eGFP per cell, and around 10 eGFP/μm^2. This is one order of magnitude below the highest levels seen during mitosis, providing an upper limit for the autofluorescence. (ii) Fluorescent proteins need to fold to their correct conformation for both maturation and fluorescence. eGFP has been engineered to fold efficiently in cells and is one of the most broadly used of all the fluorescent proteins. Refolding studies suggest that 77% of the protein can fold back into its active conformation (43). This fraction may contribute to the observation that the number of cyclin B1 molecules being 30% higher than the measured folded eGFP molecules. (iii) eGFP interactions at high concentrations changing the quantum yield—this is unlikely considering the low concentrations. Specifically, for the observed 10^5 eGFP per mitotic cell, assuming 4,000 μm^3 cell volume, corresponds to an average distance of 342 nm. Interactions are only expected for distances below 10 nm. (iv) Fluorescent protein association. eGFP is predominantly monomeric but does have a weak tendency to dimerize (44), which is not normally a problem for most imaging applications. While dimerization is not expected to change the fluorescence properties significantly, recent work has shown that in certain circumstances the molar absorbance coefficient can be enhanced on more permanent dimerization of a related GFP (45). However, this may only become a problem if the fusion partner (cyclin B1 in this case) dimerizes and brings the eGFP molecules close together in space so promote their dimerization. This is likely to be rare and can be overcome by changing the termini and/or linker sequence when fusing to eGFP.

Conclusions

We have demonstrated a simple method to quantify the number of fluorophores in cells using standard epifluorescence microscopy, and applied it to cyclin B1 expression during the cell cycle of fixed cells. We find expression levels of around 10^4 in G_1/S phase, and around 10^5 during mitosis. The method is applicable also to live cell studies, and we believe that similar studies on live cells are likely to reveal biomedically relevant information by imaging and quantifying directly the spatially resolved expression levels of proteins.

Acknowledgments

A.K. acknowledges financial support by the President's Research Scholarship programme of Cardiff University. A.M.H. acknowledges financial support by a BBSRC studentship. D.D.J. would like to thank BBSRC (BB/H003746/1 and BB/M000249/1), EPSRC (EP/J015318/1), and Cardiff SynBio Initiative/SynBioCite for supporting this work. A.M.H. was supported by a BBSRC studentship. P.B. acknowledges EPSRC for her Leadership fellowship award (grant no. EP/I005072/1). W.L. acknowledges support by a Leverhulme Royal Society Research Fellowship (grant no. LT20085). The authors thank the Cardiff School of Biosciences Protein Technology Hub for helping with production and analysis of proteins. The authors thank Iestyn Pope for assistance in the data acquisition.

Information on the data underpinning the results presented here, including how to access them, can be found in the Cardiff University data catalogue at http://doi.org/10.17035/d.2020.0107856341.

Literature Cited

1. Stephens DJ, Allan VJ. Light microscopy techniques for live cell imaging. Science 2003;300:82–86.
2. Rieder CL, Khodjakov A. Mitosis through the microscope: Advances in seeing inside live dividing cells. Science 2003;300:91–96.
3. Thorn K. A quick guide to light microscopy in cell biology. Mol Biol Cell 2016; 27(2):219–222. http://dx.doi.org/10.1091/mbc.e15-02-0088.
4. Curl CL, Bellair CJ, Harris PJ, Allman BE, Roberts A, Nugent KA, Delbridge LM. Quantitative phase microscopy - a new tool for investigating the structure and function of unstained live cells. Proc Aust Physiol Pharmacol Soc 2004;34:121.
5. Popescu G, Park Y, Choi W, Dasari MS, Ramachandra R, Feld MS, Badizadegan K. Imaging red blood cell dynamics by quantitative phase microscopy. Blood Cells Mol Dis 2008;41(1):10–16. http://dx.doi.org/10.1016/j.bcmd.2008.01.010.
6. Lee K, Kim K, Jung J, Heo J, Cho S, Lee S, Chang G, Jo Y, Park H, Park Y. Quantitative phase imaging techniques for the study of cell pathophysiology: From principles to applications. Sensors 2013;13:4170–4191.
7. Boucrot E, Kirchhausen T. Mammalian cells change volume during mitosis. PLoS ONE 2008;3(1):e1477.
8. Shribak M, LaFountain J, Biggs D, Inoue S. Quantitative orientation-independent differential interference contrast (DIC) microscopy coupled with orientation-independent polarization microscopy. Microsc Microanal 2007;13(S02):10–11.
9. Piotr Kostyk SP, Xu M. Cell cycle imaging with quantitative differential interference contrast microscopy. In: Farkas DL, Nicolau DV, Leif RC, editors. Imaging, Manipulation, and Analysis of Biomolecules, Cells, and Tissues XI, Vol. 8587. San Francisco, CA: SPIE, 2013; pp. 8587–8587-5.
10. Roukos V, Pegoraro G, Voss T, Misteli T. Cell cycle staging of individual cells by fluorescence microscopy. Nat Protoc 2015;10:334–348.
11. Hu C-K, Coughlin M, Mitchison TJ. Midbody assembly and its regulation during cytokinesis. Mol Biol Cell 2012;23:1024–1034.
12. Denk W, Strickler J, Webb W. Two-photon laser scanning fluorescence microscopy. Science 1990;248:73–76.
13. So PT. Two-photon fluorescence light microscopy. Encyclopedia of Life Sciences. 2001. https://doi.org/10.1038/npg.els.0002991.
14. Rubart M. Two-photon microscopy of cells and tissue. Circ Res 2004;95(12): 1154–1166.
15. Becker W. Fluorescence lifetime imaging - techniques and applications. J Microsc 2012;247(2):119–136.
16. Corriden R, Insel P, Junger W. A novel method using fluorescence microscopy for real-time assessment of ATP release from individual cells. Am J Physiol Cell Physiol 2007;293:1420.
17. Lippincott-Schwartz J, Patterson GH. Development and use of fluorescent protein markers in living cells. Science 2003;300:87–91.
18. Coffman VC, Wu J-Q. Counting protein molecules using quantitative fluorescence microscopy. Trends Biochem Sci 2012;37:499–506.
19. Dundr M, McNally JG, Cohen J, Misteli T. Quantitation of GFP-fusion proteins in single living cells. J Struct Biol 2002;140:92–99.
20. Wu J-Q, Pollard TD. Counting cytokinesis proteins globally and locally in fission yeast. Science 2005;310:310–314.
21. Uhlmann F. Chromosome cohesion and segregation in mitosis and meiosis. Curr Opin Cell Biol 2001;13:754–761.
22. Nebenfuhr A. Cell division control in plants. In: Verma DS, Hong Z, editors. Plant Cell Monographs, Vol. 9. Berlin, Heidelberg: Springer, 2007; pp. 195–206.
23. Imoto Y, Yoshida Y, Yagisawa F, Kuroiwa H, Kuroiwa T. The cell cycle, including the mitotic cycle and organelle division cycles, as revealed by cytological observations. J Electron Microsc 2011;60(S01):S117–S136.
24. Alberts B, Johnson A, Lewis J, Raff M, Roberts K, Walter P. Molecular Biology of the Cell, 4th ed. New York: Garland Science, 2002 (Chapter 17).
25. Vermeulen K, Van Bockstaele DR, Berneman ZN. The cell cycle: A review of regulation, deregulation and therapeutic targets in cancer. Cell Prolif 2003;36: 131–149.
26. Fisher R. Coming full circle: Cyclin-dependent kinases as anti-cancer drug targets. Subcell Biochem 2010;50:1.
27. Stewart ZA, Westfall MD, Pietenpol JA. Cell-cycle dysregulation and anticancer therapy. Trends Pharmacol Sci 2003;24:139–145.
28. Juan G, Traganos F, James WM, Ray JM, Roberge M, Sauve DM, Anderson H, Darzynkiewicz Z. Histone H3 phosphorylation and expression of cyclins A and B1 measured in individual cells during their progression through G2 and Mitosis. Cytometry 1998;32(2):71–77.
29. Griesdoorn V, Brown MR, Wiltshire M, Smith PJ, Errington RJ. Tracking the cyclin b1-GFP sensor to profile the pattern of mitosis versus mitotic bypass. Methods in Molecular Biology. New York: Springer, 2016; p. 279–285.
30. Arpino JAJ, Rizkallah PJ, Jones DD. Crystal structure of enhanced green fluorescent protein to 1.35 Å resolution reveals alternative conformations for Glu222. PLoS One 2012;7:e47132.
31. Arpino JAJ, Czapinska H, Piasecka A, Edwards WR, Barker P, Gajda MJ, Bochtler M, Jones DD. Structural basis for efficient chromophore communication and energy transfer in a constructed didomain protein scaffold. J Am Chem Soc 2012;134(33):13632–13640.
32. Patterson GH, Knobel SM, Sharif WD, Kain SR, Piston DW. Use of the green fluorescent protein and its mutants in quantitative fluorescence microscopy. Biophys J 1997;73:2782–2790.
33. Hagting A, Karlsson C, Clute P, Jackman M, Pines J. MPF localization is controlled by nuclear export. EMBOJ 1998;17(14):4127–4138.
34. Clute P, Pines J. Temporal and spatial control of cyclin B1 destruction in metaphase. Nat Cell 1999;1:82–87.
35. Smith PJ, Marquez N, Wiltshire M, Chappell S, Njoh K, Campbell L, Khan IA, Silvestre O, Errington RJ. Mitotic bypass via an occult cell cycle phase following DNA topoisomerase II inhibition in p53 functional human tumor cells. Cell Cycle 2007;6(16):2071–2081.
36. Huang J, Raff J. The disappearance of cyclin B at the end of mitosis is regulated spatially in drosophila cells. EMBO J 1999;18:2184–2195.
37. Beck M, Schmidt A, Malmstroem J, Claassen M, Ori A, Szymborska A, Herzog F, Rin-ner O, Ellenberg J, Aebersold R. The quantitative proteome of a human cell line. Mol Syst Biol 2011;7:549. https://doi.org/10.1038/msb.2011.82.
38. Terasaki M. Quantification of fluorescence in thick specimens, with an application to cyclin B-GFP expression in starfish oocytes. Biol Cell 2006;98:245–252.
39. Thomas N, Kenrick M, Giesler T, Kiser G, Tinkler H, Stubbs S. Characterisation and gene expression profiling of a stable cell line expressing a cell cycle GFP sensor. Cell Cycle 2005;4:191–195.
40. Frisa PS, Jacobberger JW. Cell cycle-related cyclin B1 quantification. PLoS One 2009;4:e7064.
41. Xu N, Chang DC. Different thresholds of MPF inactivation are responsible for controlling different mitotic events in mammalian cell division. Cell Cycle 2007;6: 1639–1645. pMID: 17598982.
42. Arooz T, Yam CH, Siu WY, Lau A, Li KKW, Poon RYC. On the concentrations of cyclins and cyclin-dependent kinases in extracts of cultured human cells. Biochemistry 2000;39:9494–9501.
43. Arpino JA, Reddington SC, Halliwell LM, Rizkallah PJ, Jones DD. Random single amino acid deletion sampling unveils structural tolerance and the benefits of helical registry shift on GFP folding and structure. Structure 2014;22(6):889.
44. Shaner NC, Steinbach PA, Tsien RY. A guide to choosing fluorescent proteins. Nat Methods 2005;2:905–909.
45. Worthy HL, Auhim HS, Jamieson WD, Pope JR, Wall A, Batchelor R, Johnson RL, Watkins DW, Rizkallah P, Castell OK. Positive functional synergy of structurally integrated artificial protein dimers assembled by Click chemistry. Commun Chem 2019;2:83.